OPEN

High-temperature thermoelectric transport at small scales: Thermal generation, transport and recombination of minority carriers

Gokhan Bakan, Niaz Khan, Helena Silva & Ali Gokirmak

Department of Electrical and Computer Engineering, University of Connecticut, Storrs, CT 06269-4157, USA.

Correspondence and
requests for materials
should be addressed to
A.G. (gokirmak@engr.
uconn.edu)

Thermoelectric transport in semiconductors is usually considered under small thermal gradients and when it is dominated by the role of the majority carriers. Not much is known about effects that arise under the large thermal gradients that can be established in high-temperature, small-scale electronic devices. Here, we report a surprisingly large asymmetry in self-heating of symmetric highly doped silicon microwires with the hottest region shifted along the direction of minority carrier flow. We show that at sufficiently high temperatures and strong thermal gradients ($\sim$1 K/nm), energy transport by generation, transport and recombination of minority carriers along these structures becomes very significant and overcomes convective energy transport by majority carriers in the opposite direction. These results are important for high-temperature nanoelectronics such as emerging phase-change memory devices which also employ highly doped semiconducting materials and in which local temperatures reach $\sim$1000 K and thermal gradients reach $\sim$10–100 K/nm.

Scaling of electronic devices has so far resulted in tremendous improvements in computation speed and data storage capacity at significantly reduced cost and power[1]. Scaling to the 10 nm regime is enabling alternative device technologies such as phase-change memory[2] and other nanoscale resistive memory devices which utilize local electrothermal processes to induce reversible changes to a small volume of material for non-volatile data storage or computation. These devices, complementing conventional CMOS, can lead to a new wave of breakthroughs in electronics if the behaviour of materials at small scale and local high-temperature electrothermal processes are well understood. Until recently, electrothermal phenomena have been almost exclusively studied in the context of thermoelectric energy conversion or solid-state cooling[3] using large-scale devices and at relatively small thermal gradients. In contrast, electronic transport has been studied at small scales for a long time, but in the lower temperature range ($<$400 K) and under negligible thermal gradients. Here we show the significance of thermoelectric effects for high-temperature electronics through self-heating of lithographically-defined symmetric microwires which consistently start melting at one end. This extreme asymmetry in melting reveals the significance of energy transport by thermal generation of minority carriers, their transport and recombination downstream. This thermal transport mechanism has strong implications for novel nanoscale electronic devices that utilize electrothermal processes to change the material state for their operation.

Results

Self-heating through microsecond voltage pulses. The experiments presented here are performed on highly doped ($n \sim 6 \times 10^{19}$ cm^{-3}) silicon microwires which are self-heated to high temperatures (Figure 1a). These wires with large contact extensions were lithographically defined on a nanocrystalline silicon (nc-Si) thin film using an i-line stepper and reactive ion etching. The underlying SiO$_2$ layer was partially removed, suspending the wires between the contact-extensions anchored to the substrate. Tungsten probes were used to make electrical contact at these large extension regions. Extremely asymmetric partial melting of these symmetric nc-Si wires (T$_{melt} \sim$ 1690 K) is observed close to the lower potential end of the wires for 30 V, 1 μs pulses (Figure 1b, c). Higher voltage pulses ($\sim$40 V) completely melt (Figure 1d), thin (Figure 1e) and eventually break the wires depending on the pulse durations (Figure 1f). These results suggest that melting consistently starts from the lower potential end (see supplementary note 1), however it is not possible to capture the evolution of the thermal profiles in these
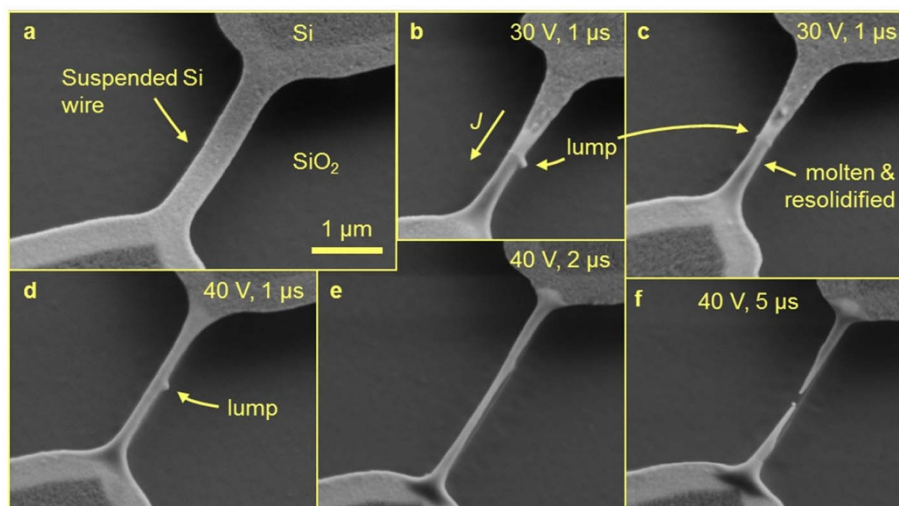
Figure 1 | SEM images of suspended *n-type* Si wires (thickness: 50 nm). (a) An as-fabricated and (b–f) five wires pulsed using indicated durations and amplitudes. Moderately pulsed wires (J ~ 2–7 MA/cm²) (b–c) show melting on the source side, whereas larger amplitude pulses (d–f) result in complete melting, sagging and breaking.

experiments. In order to verify these results using an alternative approach and validate the electrothermal models that will be used to analyse the results, we have performed experiments on *n-* and *p-type* microwires using lower-amplitude low-frequency AC signals and observed the profile of the emitted light.

Self-heating through low frequency AC signals. These microwires can be self-heated to sufficiently high temperatures to observe black-body radiation in the visible range without melting or breaking (Figure 2) using lower amplitude (J ~ 2 MA/cm²) electrical signals. The emitted light is captured at 30 frames/second using a commercial digital camera mounted on a microscope to obtain emission profiles of the structures. The use of AC signals (~1 Hz,) allows verification of structural integrity through consistency in repeated cycles, and eliminates the need to determine the wire

centre as the reference point. The emitted light intensity, hence the hottest spot, is consistently higher on the terminal where the majority carriers enter the wire for both *n-* and *p-type* wires, in agreement with the pulse experiments. The polarity of the thermal profiles in these experiments is opposite of what would be expected in a metal experiencing electronic-convective heat flow. The surprisingly large degree of asymmetry (Figure 1b, c) points to dominance of a distinct thermal transport mechanism in semiconductors experiencing high temperatures and strong thermal gradients.

Discussion

The polarity of the asymmetry – hottest point being closer to the source of the majority charge carriers entering the wire– is in agreement with observations on other self-heated semiconductor structures such as silicon microstructures and PCM nano-bridges[4,5].
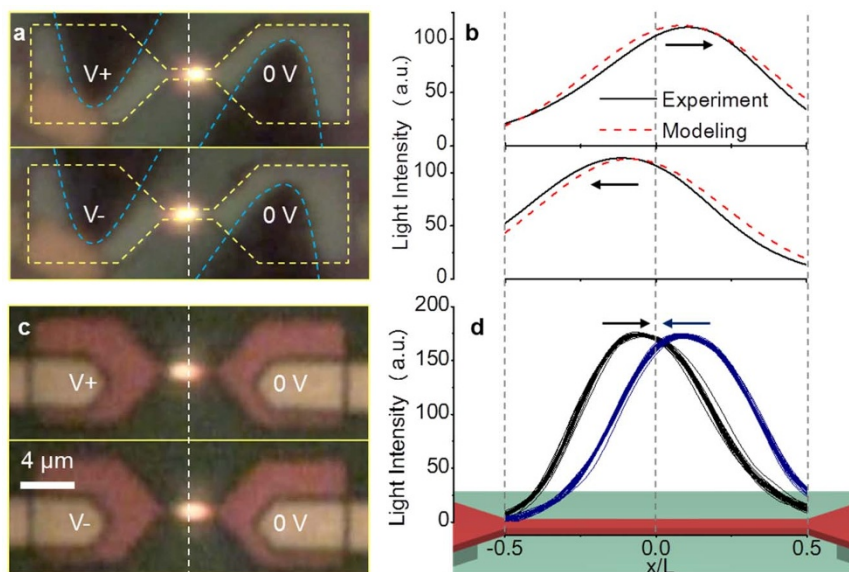

Figure 2 | Light emission from Si microwires. (a) Optical images of a 2.5 µm long, suspended, *n-type* wire (thickness: 80 nm) biased with shown voltage polarities (J ~ 2.6 MA/cm²). Geometries enclosed with dashed lines indicate the edges of the Si structures and metal probes. (b) Averaged light intensity profiles along the *n-type* wire for each direction of current compared to simulated light intensity profiles. (c) Optical images of a 4 µm long, suspended, *p-type* wire (thickness: 120 nm, J ~ 1.7 MA/cm²). (d) Light intensity profiles along the *p-type* wire for both direction of current (30 curves per polarity). Arrows indicate current directions. 3D drawing of a wire is shown at the bottom. Vertical dashed lines indicate the wire centres and ends.

While the asymmetry has been attributed to thermoelectric Thomson heat[4,5], no explanation has been given to the underlying physical phenomena giving rise to this behaviour. In order to understand the electrothermal phenomena in these self-heated microwires, we have revisited the general formulations for electrical and thermal transport in current carrying structures and commonly known thermoelectric effects. The thermoelectric effects, Seebeck and Peltier effects due to junctions of two different materials, and Thomson effect (heat) in uniform materials experiencing a thermal gradient and electric current, are the results of the energy exchange between the charge carriers and the lattice[6]. The average energy of a charge carrier is defined as the Peltier coefficient $\Pi(T)$ multiplied by the elementary charge (q). $\Pi(T)$ is the product of the Seebeck coefficient $S(T)$ of the material and the local temperature. Strong $\Pi(T)$ gradients lead to increased energy exchange between the carriers and the lattice as the carriers move along the temperature gradient (large Thomson effect).

The electrical current density can be expressed as the sum of drift and diffusion components: $J = J_{Drift} + J_{Diff}$. The drift current is due to the electric field (E) acting on the carriers and the diffusion current comes into existence due to gradients in carrier concentrations (n) and their velocities (diffusivities, D). The general forms (in linear approximation) for these components are[7]:

$$ J = \overbrace{\sigma E}^{J_{Drift}} + \overbrace{q\nabla(Dn)}^{J_{Diffusion}} = \sigma E + qn\nabla D + qD\nabla n, \quad (1) $$

where σ is electrical conductivity. If the material is uniform, as in our case, temperature gradient is the only driver for diffusion of charge carriers. Hence, the diffusion current can be modelled in terms of temperature gradient and temperature derivatives of D and n:

$$ J_{Diffusion} = \underbrace{q(n\frac{dD}{dT} + D\frac{dn}{dT})}_{-\sigma S}\nabla T \quad (2) $$

Open-circuit analysis shows that the diffusion coefficient in the above expression is the Seebeck coefficient (S = $-\Delta V/\Delta T$) scaled with electrical conductivity of the material. Hence, the diffusion term in the electronic drift-diffusion model in a uniform material experiencing a thermal gradient is reduced to $-\sigma S\nabla T$[8]:

$$ \nabla\cdot J = \nabla\cdot(\overbrace{-\sigma\nabla V}^{Drift}\overbrace{-\sigma S\nabla T}^{Diffusion}) = 0. \quad (3) $$

The temperature change in the wire can be modelled by accounting for Joule heating, heat conduction through the lattice and heat transport by charge carriers (Thermoelectric heat)[8]:

$$ \underbrace{dC_P\frac{dT}{dt}}_{\substack{heat\ absorbed\\by\ material}} - \underbrace{\nabla\cdot(k\nabla T)}_{\substack{heat\ loss\\through\\conduction}} = \underbrace{-\nabla V\cdot J}_{\substack{Joule\\heating}} \underbrace{-\nabla\cdot(J\Pi)}_{\substack{Thermoelectric\\heat}}, \quad (4) $$

where d is the mass density, C_P is the specific heat, and k is the thermal conductivity.

The thermoelectric heat term can be broken down as the electron and hole contributions[9,10]:

$$ -\nabla\cdot(J\Pi) = -\nabla\cdot(J_e\Pi_e + J_h\Pi_h) $$
$$ = -[J_e\cdot\nabla(\Pi_e) + J_h\cdot\nabla(\Pi_h) + \Pi_e\nabla\cdot J_e + \Pi_h\nabla\cdot J_h], \quad (5) $$

where the subscripts for J and Π refer to the respective carrier type (electrons or holes). Since each generation event results in one electron and one hole, and the total electrical current is constant, net generation rate is $\nabla\cdot J_h = -\nabla\cdot J_e$. Rearranging equation (5) to a more intuitive form leads to *electronic-convective heat transfer* and *generation-transport-recombination* (*GTR*) terms appearing as the two distinct components of thermoelectric heat:

$$ \underbrace{-\nabla\cdot(J\Pi)}_{\substack{Thermoelectric\\heat}} = \underbrace{\overbrace{-J_e\cdot\nabla(\Pi_e)}^{by\ e^-}\overbrace{-J_h\cdot\nabla(\Pi_h)}^{by\ h^+}}_{\substack{electronic-convective\\heat\ transfer}} $$
$$ -\underbrace{\overbrace{\nabla\cdot J_h}^{\substack{net\\generation\\rate}}\overbrace{(\Pi_h - \Pi_e)}^{\substack{energy\ of\\an\ e^--h^+\ pair}}}_{\substack{generation-(transport)-\\recombination\ heat}} \quad (6) $$

The electronic-convective heat transfer is due to carriers moving in a thermal profile exchanging energy with their surroundings (Figure 3a).
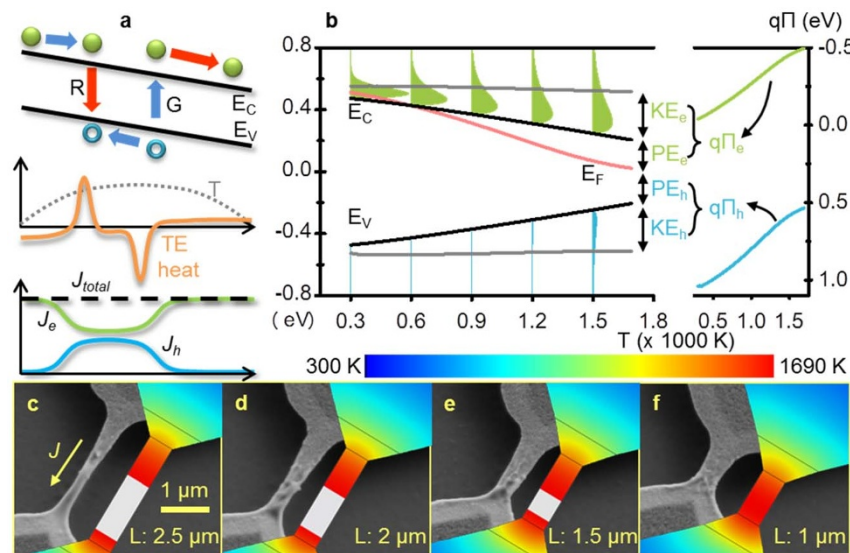

Figure 3 | Thermoelectric effects in Si microwires. (a) A simplified illustration of carrier flow and the thermoelectric heat transfer on energy-band diagram of an electrically biased wire due to: 1) generation and recombination and 2) electronic-convective mechanisms. (b) Calculated energy-band diagram of 6×10^{19} cm^{-3} doped *n-type* Si with electron and hole distributions from 300 to 1500 K and temperature dependent Peltier coefficients of electrons (Π_e) and holes (Π_h). (c–f) Partially crystallized wires (thickness: 50 nm) with indicated lengths after 30 V, 1 µs pulse ($J \sim 2$–7 MA/cm^2), and corresponding simulated temperature profiles (white > T$_{melt}$ = 1690 K). The current direction is indicated in (c).

In highly doped silicon, average energy (kinetic energy + chemical potential energy) of electrons ($q\Pi_e = KE_e + PE_e$) increases with temperature. Hence, electrons absorb energy as they climb the temperature profile and release energy on their way down. Average energy of holes ($q\Pi_h$) decreases with temperature as the Fermi level moves from above the conduction band edge towards the mid-gap (Figure 3b) due to the large number of thermally generated carriers at high temperatures (see supplementary note 3). Hence, energy absorption/release due to the flow of holes is in the same direction of that of electrons. Even though the average energy transported by holes is very large compared to that of electrons, their overall contribution is very small owing to their small numbers. The *GTR* term is due to energy absorption associated with electron-hole pair generation, their separation by the electric field and heat release due to their recombination elsewhere (Figure 3a). The electronic-convective and *GTR* terms compete on the wire. The polarity of our experimental results indicates that *GTR* is the dominant mechanism.

We have performed 3D finite element simulations of the n-type nc-Si wires by solving equation (3) and (4) self-consistently, compared them to the experimental results (Figure 3c–f), evaluated the relative contributions of the thermoelectric components as identified in equation (6). The simulation results show a significant asymmetry in heating and melting with the peak temperature shifted in the direction of the minority carriers flow, as observed in the experiments. The molten portions of the simulated wires vary from 30 to 50% (for L = 1.5 to 2.5 μm) of wire length, comparable to the observed molten and crystallized ratios in the experiments (see supplementary note 9). Our model, which neglects deviations from equilibrium carrier concentrations (calculated using equilibrium Fermi distribution) due to carrier flow and uses Seebeck coefficient based on measurements and calculations assuming mild temperature gradients, seems to capture the general behaviour in the pulse experiments with small discrepancies.

In order to compare the simulated thermal profiles with optical observations using long duration AC signals, we have calculated the expected black-body radiation profile in the visible range (for $T_{peak} = 1640$ K). We have assumed that the wire consists of many small light sources with Gaussian light profiles to model the diffraction limit of the optics used in the experimental setup[11]. The simulated and experimental radiation intensity profiles are in good agreement, with the observed experimental asymmetry being slightly stronger (Figure 2), verifying the models used to calculate the thermal profiles.

The asymmetry in the thermal profile is observed to be larger for shorter wires, possibly due to increased thermal gradients (~1 K/nm) and electric field. Hence the impact of the thermoelectric contributors is more significant at smaller geometries. Individual evaluation of the *GTR* and the *electronic-convective* terms shows that the *electronic-convective* contribution is stronger until significant thermal generation starts taking place (T > 1300 K for Si) after which *GTR* dominates.

In summary, charge carriers exchange energy (thermalize) with their environment and their drift by an electric field gives rise to net thermal transport at junctions of two dissimilar materials (Peltier Heat) or within a single material experiencing a thermal gradient (Thomson Heat). Thomson heat in metals is dominated by convective heat flow by the charge carriers whose total energy $q\Pi(T)$ varies as a function of temperature. In semiconductors, thermal carrier generation (energy absorption) and recombination (energy release) processes contribute to Thomson heat as well: in the presence of an electric field, the thermally generated electrons and holes are separated, and thermal energy is transported from regions of net carrier generation to regions of net recombination. In uniformly doped semiconductors, the concentration of minority carriers determines the recombination rate and their drift determines the thermoelectric heat flow associated with the *generation-transport-recombination* (*GTR*) process. The *GTR* contribution, in the direction of minority

carrier drift, competes with the electronic-convective heat flow, in the majority carrier drift direction. *GTR* becomes the dominant component of Thomson heat in highly doped semiconductors experiencing elevated temperatures and strong thermal gradients, as in the case of the Si microwires demonstrated here. Local self-heating to high temperatures leads to extreme thermal gradients (~1 K/nm in our experiments and >10 K/nm expected in PCM devices[5,12]) which give rise to significant gradients in band-gap, kinetic energy, and minority and majority carrier concentrations, all of which contribute to strong thermal and thermoelectric transport. Hence, semiconductors have a significant thermal transport mechanism due to generation-transport-recombination of free charge carriers (at temperatures where thermal generation becomes significant) in addition to electronic and phonon contributions which dominate in metals and insulators. This additional mechanism is very sensitive to electric fields, giving rise to significant thermoelectric response. As electro-thermal transport at high-temperatures and small scales becomes more industrially relevant with the emergence of phase-change memory[12] and other nanoscale resistive non-volatile memories[13,14], design considerations have to include the impact of electrothermal transport due to GTR in the semiconducting elements.

Methods

Device fabrication. The microwires were patterned on *n*- and *p*-type nc-Si films deposited on oxidized single crystal Si wafers (~500 nm SiO_2) in a low pressure chemical vapour deposition (LPCVD) system at 580 C or 600 C with phosphorous doping or at 560 C with boron doping ([P], [B] > 10^{20} cm^{-3}). The films are a few times thicker than the average grain size (the grain size distribution is estimated to be 10 ~ 50 nm based on the scanning electron micrographs). No preferred grain orientation is expected. The wires were suspended by etching the underlying oxide using buffered oxide etch. The wires' dimensions range from 0.5 to 5.5 μm in length and 100 nm to 1 μm in width. Metal extensions (Ti/Ni or Ti/Al stacks) were deposited to form ohmic contacts on some of the samples.

Electrical measurements. The room temperature resistivity of the *n-type* films is in the range of 20–23 mΩ.cm and the resistivity of the *p-type* film is 13 mΩ.cm. Electron concentration and Hall mobility of the *n-type* films are measured as $(6 \pm 2) \times 10^{19}$ cm^{-3} and 4.4 ± 1.5 cm^{2}V^{-1}s^{-1}. Hall measurements of the films suggest that only a fraction (~10%) of the dopants is activated at room temperature. The experiments were conducted using a semiconductor probe station, a parameter analyser, a pulse generator unit, and an oscilloscope. The oscilloscope was used to measure the applied voltage (V_{Pulse}) and current (by measuring voltage across the 50 Ω termination resistor (V_S) in series with the wire) for some of the experiments. Tungsten needles were used to probe the metal contacts or the Si contact regions of wires without metal extensions. Room temperature resistance was extracted from low voltage *I-V* characteristics of the wires (0–1 V). The observed linear behaviour suggests reliable Ohmic contacts and negligible self-heating. A commercial HD camera (Sony Handycam®) was used to capture light emission from the wires biased with low frequency ac signals (0.5–1 Hz using a signal generator). The captured light emission videos were stabilized and then analysed to extract light intensity profiles using MATLAB.

Numerical modelling. In these simulations, we assume that the charge carriers remain in local thermal equilibrium with the lattice ($T_{electron} = T_{lattice}$) and use an effective medium approximation, neglecting the impact of individual grain boundaries. The geometries used for the modelling is kept as small as possible to reduce the complexity of the simulations without affecting the heat generation and diffusion mechanisms. The thermal boundary conditions are set as 300 K at the bottom of the Si substrate, 5 μm below the SiO_2-Si interface, and on the 1 μm radius contacts 5 μm away from the wire ends. To account for the contact pad resistance between where the actual probes are located in the experiments and what is used for the modelling, a 19 kΩ resistor in series with the wire is included in the model. Temperature dependent material parameters (σ, k, C_P, S) are used in for modelling. ρ, k and S of nanocrystalline thin films depend on deposition conditions and are not easy to measure directly at elevated temperatures. We have measured $\rho(T)$ and $S(T)$ simultaneously in the 300–650 K range and extracted $k(T)$ in this range by using the measured $\rho(T)$ and matching simulated and experimental *I-V* curves[15]. We have extrapolated $k(T)$ and extracted $\rho(T)$ beyond 650 K using the same approach. This method effectively accounts for the expected reduction in $k(T)$ due to ballistic or non-local transport under extreme thermal gradients[16]. $S(T)$ beyond 650 K is extrapolated based on calculations for single-crystal silicon (x-Si) using the Boltzmann transport model and Fermi-Dirac statistics. The latent heat of fusion of Si during the solid-to-liquid phase transition is accounted for by incorporating a 10 K wide peak in C_P around melting temperature where all the material parameters linearly transition to their liquid-state values. The liquid state ρ_{liquid}, k_{liquid} and S_{liquid} values are obtained from the

literature (see Supplementary Figure S2 for all the physical parameters used in the simulations).

1. Peercy, P. S. The drive to miniaturization. *Nature* **406**, 1023–1026 (2000).
2. Lankhorst, M. H. R., Ketelaars, B. W. & Wolters, R. Low-cost and nanoscale non-volatile memory concept for future silicon chips. *Nature Materials* **4**, 347–352 (2005).
3. DiSalvo, F. J. Thermoelectric cooling and power generation. *Science* **285**, 703–706 (1999).
4. Mastrangelo, C. H., Yeh, J. H. J. & Muller, R. S. Electrical and optical characteristics of vacuum-sealed polysilicon microlamps. *IEEE Trans. Electron Devices* **39**, 1363–1375 (1992).
5. Castro, D. T. *et al.* Evidence of the thermo-electric thomson effect and influence on the program conditions and cell optimization in phase-change memory cells. *IEDM Tech. Dig.* 315–318 (2007).
6. Rowe, D. M. in *Thermoelectrics Handbook: Macro to Nano* (eds Rowe, D. M.) (CRC Press, 2006).
7. Van Zeghbroeck, B. *Principles of Semiconductor Devices [Online]* (2002), http://ecee.colorado.edu/~bart/book, (Date of access: 02/04/2013).
8. Landau, L. D., Lifshitz, E. M. & Pitaevskii, L. P. in *Electrodynamics of Continuous Media* 2nd edn (Butterworth-Heinemann, 1984).
9. Wachutka, G. K. Rigorous thermodynamic treatment of heat generation and conduction in semiconductor device modeling. *IEEE Trans. Computer-Aided Design* **9**, 1141–1149 (1990).
10. Lindefelt, U. Heat generation in semiconductor devices. *J. Appl. Phys.* **75**, 942–957 (1994).
11. Bakan, G. *et al.* Self-heating of silicon microwires: Crystallization and thermoelectric effects. *J. Mater. Res.* **26**, 1061–1071 (2011).
12. Choi, Y. *et al.* A 20 nm 1.8 V 8 Gb PRAM with 40 MB/s program bandwidth. *ISSCC Tech. Dig.* 46–48 (2012).
13. Waser, R. & Aono, M. Nanoionics-based resistive switching memories. *Nature Mater.* **6**, 833–840 (2007).
14. Waser, R., Dittmann, R., Staikov, G. & Szot, K. Redox-Based resistive switching Memories–Nanoionic mechanisms, prospects, and challenges. *Adv. Mater.* **21**, 2632–2663 (2009).
15. Bakan, G., Adnane, L., Gokirmak, A. & Silva, H. Extraction of temperature dependent electrical resistivity and thermal conductivity from silicon microwires self-heated to melting temperature. *J. Appl. Phys.* **112**, 063527 (2012).
16. Chen, G. Ballistic-diffusive heat-conduction equations. *Phys. Rev. Lett.* **86**, 2297–2300 (2001).

Author contributions

G.B. did experiments (device fabrication, electrical and optical characterization and SEM imaging) and analysis and computational studies. N.K. did experiments and analysis related to the optical observations of the heating asymmetry. H.S. worked on the analysis and computational studies. A.G. did experiments (device fabrication, electrical and optical characterization and SEM imaging) and analysis. G.B., H.S. and A.G. worked on the preparation of the manuscript.

Additional information